Control of vacuole membrane homeostasis by a resident PI-3,5-kinase inhibitor

PC Malia[a], Johannes Numrich[a], Taki Nishimura[b], Ayelén González Montoro[a], Christopher J. Stefan[b], and Christian Ungermann[a,1]

[a]Biochemistry Section, Department of Biology/Chemistry, University of Osnabrück, 49076 Osnabrück, Germany; and [b]Medical Research Council Laboratory for Molecular Cell Biology, University College London, WC1E 6BT London, United Kingdom

Edited by William T. Wickner, Geisel School of Medicine at Dartmouth College, Hanover, NH, and approved March 23, 2018 (received for review December 27, 2017)

Lysosomes have an important role in cellular protein and organelle quality control, metabolism, and signaling. On the surface of lysosomes, the PIKfyve/Fab1 complex generates phosphatidylinositol 3,5-bisphosphate, PI-3,5-P_2, which is critical for lysosomal membrane homeostasis during acute osmotic stress and for lysosomal signaling. Here, we identify the inverted BAR protein Ivy1 as an inhibitor of the Fab1 complex with a direct influence on PI-3,5-P_2 levels and vacuole homeostasis. Ivy1 requires Ypt7 binding for its function, binds PI-3,5-P_2, and interacts with the Fab1 kinase. Colocalization of Ivy1 and Fab1 is lost during osmotic stress. In agreement with Ivy1's role as a Fab1 regulator, its overexpression blocks Fab1 activity during osmotic shock and vacuole fragmentation. Conversely, loss of Ivy1, or lateral relocalization of Ivy1 on vacuoles away from Fab1, results in vacuole fragmentation and poor growth. Our data suggest that Ivy1 modulates Fab1-mediated PI-3,5-P_2 synthesis during membrane stress and may allow adjustment of the vacuole membrane environment.

Ivy1 | Fab1 | IBAR | lysosome | osmotic stress

Eukaryotic cells have a specialized endomembrane system of interconnected organelles with specific membrane and protein compositions, which have to be adjusted in response to alterations in metabolism or during stress. These adjustments follow different time scales. Alterations in lipid composition requires, apart from sensing and signaling, synthesis and transport of missing components, whereas posttranslational modifications of lipids or proteins will occur immediately, once a signal has been received. Phosphoinositides (PIP) are a particular class of lipids, which are rapidly modified by kinases and phosphatases (1). These lipids mark organelles and provide specific binding surfaces for peripheral membrane proteins. They function together with organelle-specific membrane proteins such as Rab GTPases as a coincidence detection code to recruit proteins to membranes (2).

Within the endolysosomal system, PIP lipids determine the fate of endosomes and vacuoles (lysosomes in metazoan). In particular, phosphatidylinositol-3-phosphate (PI-3-P) is generated by Vps34 complexes and regulates cargo sorting, endosome positioning, dynamics, and maturation, but also autophagy (3). At vacuoles, PI-3-P is further phosphorylated to phosphatidylinositol-3,5-bisphosphate (PI-3,5-P_2), which has been implicated in protein sorting, regulation of vacuolar ion channels, and activation of the target of rapamycin complex I (TORCI) (4–7). Studies in yeast revealed that PI-3,5-P_2 levels have a tight connection to the cellular response to osmotic stress. In normal medium, PI-3,5-P_2 amounts are very low, although they increase strongly if cells are exposed to hypertonic stress (8). This PI-3,5-P_2 increase results in fragmentation of vacuoles to compensate for the loss of its volume while maintaining its membrane (9). PI-3,5-P_2 effectors are likely involved in the regulation of vacuole membrane homeostasis (6, 7). In agreement with its central role for vacuolar and cell physiology, defects in its synthesis results in severe neurodegenerative diseases in humans (10–13).

PI-3,5-P_2 synthesis at vacuoles and lysosomes requires a complex, consisting of the Fab1 kinase (PIKfyve in humans), the integral membrane protein Vac7, the PI-3,5-phosphatase Fig4, Vac14, and Atg18 (8, 14–19). Vac14 acts as a scaffolding protein linking the remaining subunits together (20, 21). Mutational analysis revealed that Fig4, Vac7, and Vac14 are required for full Fab1 activity, while Atg18 might function as a Fab1 inhibitor (21–23). As Fab1 is found on the vacuole-like lysosome, membrane stress might be a direct activator of Fab1, yet molecular mechanisms that control Fab1 activity are lacking.

We recently identified Ivy1 as an inverted BAR (I-BAR) protein that localizes to yeast vacuoles and affects vacuole membrane homeostasis. Ivy1 is recruited by Rab7-like Ypt7 to the vacuole and colocalizes with the TORC1-activating EGO complex at defined, dot-like structures along the vacuole membrane (24). Here, we now provide a molecular explanation of Ivy1 function. We show that Ivy1 binds and inhibits the Fab1 complex and, thus, regulates vacuolar PI-3,5-P_2 levels. Membrane stress results in a local separation of Ivy1 from Fab1 on the vacuole membrane, in subsequent Fab1 hyperactivity and upregulation of PI-3,5-P_2 levels, and consequently vacuole fission and TORC1 signaling.

Results

A Critical Role of Ypt7 Binding for Ivy1 Function. We previously postulated that Ivy1 might affect vacuole membrane homeostasis, potentially by its I-BAR domain (24). Localization of Ivy1 to vacuoles involves PIP lipids and Ypt7 (24). To understand the contributions of the I-BAR domain and Rab binding for Ivy1 function, we searched for the minimal domain within Ivy1 and traced GFP-tagged Ivy1 fragments by colocalization with FM4-64–stained vacuoles. N- and C-terminal segments outside of the I-BAR domain were dispensable for Ivy1-GFP localization (Fig. 1 *A*, *a* vs. *b*).

Significance

The lysosome-like vacuole is the main organelle to degrade membrane proteins and organelles and, thus, provides amino acids, but also ions to the cytosol for cellular survival. Maintenance of vacuole membrane integrity is thus important for cellular adaptations. The vacuole contains several protein complexes on its surface to maintain the vacuole functional, and one such complex is a lipid kinase named Fab1 (of PIKfyve in human cells). Fab1 is part of a protein complex that produces a phosphorylated lipid, PI-3,5-P_2. Other proteins bind PI-3,5-P_2 and can fragment the vacuole to balance volume vs. membrane during stress. We now identify Ivy1 as a protein that binds Fab1 and controls its activity.

Author contributions: P.C.M., J.N., A.G.M., C.J.S., and C.U. designed research; P.C.M., J.N., and T.N. performed research; P.C.M., J.N., T.N., A.G.M., C.J.S., and C.U. analyzed data; and P.C.M., A.G.M., C.J.S., and C.U. wrote the paper.

The authors declare no conflict of interest.

This article is a PNAS Direct Submission.

[1]To whom correspondence should be addressed. Email: cu@uos.de.

This article contains supporting information online at www.pnas.org/lookup/suppl/doi:10.1073/pnas.1722517115/-/DCSupplemental.

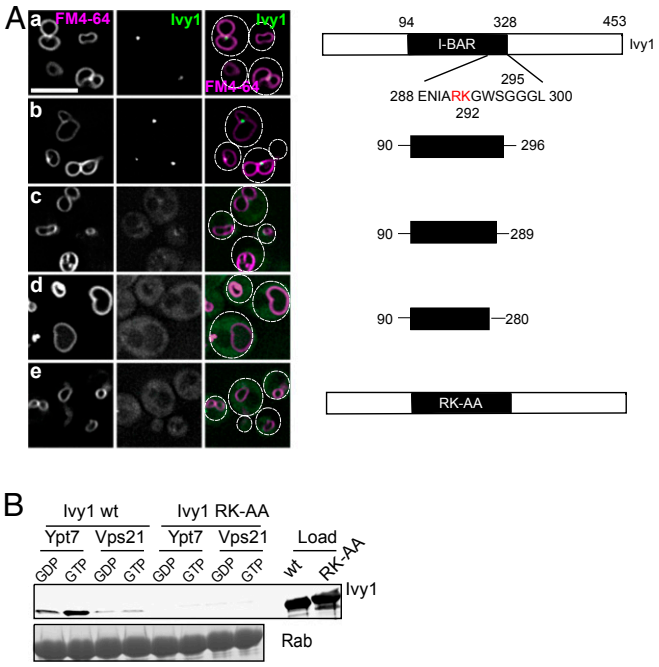

Fig. 1. Mapping Ypt7 interaction site in Ivy1 and its functional relevance. (*A*) Ivy1 mutant's localization in vivo. *ivy1*Δ cells expressing indicated Ivy1-GFP proteins under the control of the *IVY1* promoter were monitored by fluorescence microscopy. Vacuoles were stained with FM4-64 (*Materials and Methods*). (Scale bar: 5 μm.) (*B*) Impaired Ypt7 binding of the Ivy1 RK-AA mutant protein. Recombinant His-Ivy1 or RK-AA mutant was incubated with GST-Rabs, preloaded with GDP or GTPγS, and immobilized in GSH beads. Bound proteins were eluted, TCA precipitated, and analyzed by Western blotting. Beads were boiled to elute Rabs. Proteins were resolved on SDS gels and stained with Coomassie.

Further deletion of a segment of seven residues close to the end of the Ivy1 I-BAR domain abolished vacuole localization (Fig. 1 *A*, *c* and *d*). Within this targeting region, we mutated two prominent positively charged residues (RK) to alanine. The resulting RK-AA mutant was cytosolic (Fig. 1 *A*, *e*), and we thus addressed effects on Ypt7 and PIP lipid binding affinities. Using established Rab protein binding assays (25), recombinant Ivy1 RK-AA was not able to bind GST-Ypt7 in vitro, whereas wild-type Ivy1 was specifically retained by Ypt7-GTP (Fig. 1*B*). In contrast, Ivy1 and the RK-AA mutant protein retained PIP lipid binding properties. Purified Ivy1 and the RK-AA mutant bound to PI-3-P and PI-3,5-P_2 in liposome flotation assays, whereas binding to phosphatidic acid, PI, or PI-4-P was negligible (Fig. S1*A*). Together, these results point to a critical role for the I-BAR domain in Ivy1 vacuolar localization and suggest that the RK-AA mutant protein is specifically impaired in Ypt7 binding rather than generally misfolded (Fig. S1*B*).

To determine whether Ypt7 binding or vacuole localization is critical for Ivy1 function, we relocalized the RK-AA mutant to vacuoles via a GFP-specific chromobody (CB) that was attached to the vacuolar Ego1 protein (Fig. S1*C*). Although the RK-AA mutant was now on vacuoles (Fig. S1*C*), it was not able to complement the previously reported vacuolar morphology defect or synthetic growth defect of *ivy1*Δ *vma16*Δ mutant cells on rapamycin, an inhibitor of TORC1 (Fig. S1 *C* and *D*) (24). Thus, Ypt7 binding and Ivy1 function are intimately linked.

Ivy1 Affects Vacuole Membrane Homeostasis. As Ivy1 binds PI-3,5-P_2 and redistributes along vacuolar membranes during alterations in PI-3,5-P_2 concentrations (Fig. S1*A*) (24), we explored its role in PI-3,5-P_2–mediated vacuole fragmentation as a response to osmotic stress. To test if Ivy1 levels affect the response of cells to high salt, we overexpressed the protein and scored vacuole fragmentation. Remarkably, cells overexpressing Ivy1 were largely resistant to vacuole fragmentation (Fig. 2 *A* and *B*). Moreover, overexpression using the *TEF* promoter did not impair Ypt7 function as vacuoles remained round under these conditions. As a direct demonstration, we coincubated wild type and cells overexpressing Ivy1 in a flow chamber and rapidly exposed cells to high salt. Wild-type cells responded in seconds with vacuole fragmentation, whereas Ivy1-overexpressing cells maintained round vacuoles (Fig. 2*C*). This observation was independent of the strain used for tracing vacuole morphology.

Surprisingly, normal round vacuoles have been observed in *ivy1*Δ cells (24, 26). We speculated that Ivy1 might carry out an essential function in vacuole membrane homeostasis, and existing *ivy1*Δ mutant strains might carry suppressors masking the phenotype of the deletion. To test this, we mated two wild-type strains that were transformed with a centromeric plasmid with a *URA3* marker coding for *IVY1*. We deleted *IVY1* in those cells, sporulated them, and dissected the tetrads. Resulting haploid spores grew normally as the *ivy1* deletion was still complemented by the plasmid-encoding *IVY1* wild type. This changed drastically when cells were treated with 5-fluoro-orotic acid (5-FOA), which only allows those cells to survive that lost the *URA3*-encoding plasmid. Cells lacking *IVY1* now had fragmented vacuoles (Fig. 2 *G* and *H*) and grew more slowly (Fig. 2*I*). Having achieved a clean *ivy1Δ* mutant, we searched for the minimal functional fragment of Ivy1. We transformed our *ivy1Δ* strain with the protecting pRS416-*IVY1* plasmid with a second centromeric plasmid with a *LEU2* marker that either encoded full-length Ivy1 or corresponding truncation mutants and scored the growth defects in 5-FOA (Fig. S2*D*). Only full-length Ivy1 completely rescued the growth defect of the *ivy1Δ* mutant. The N-terminal part seemed to be particularly relevant for Ivy1 function, since it was the only truncation that partially rescued the growth defect. Importantly, the RK-AA mutant had severe problems to grow, indicating that Ivy1 required the interaction with Ypt7 to fulfill its function (Fig. 1). To find further support that the loss of Ivy1 affects vacuole homeostasis, we tagged Ivy1 with a C-terminal auxin-induced degron (AID) tag (27). Cells with Ivy1-AID lost the protein within 30 min after indol acetic acid (IAA) addition. By tracing vacuole morphology, we observed in parallel progressive fragmentation of cells with depleted Ivy1, whereas wild-type cells maintained round vacuoles (Fig. S2 *A* and *B*).

Our data so far is consistent with an inhibition of vacuole fragmentation by Ivy1 and suggest that Ivy1 might inhibit Fab1 PI-3-P 5-kinase activity. To test this, we initially measured PI-3,5-P_2 levels in control and cells overexpressing Ivy1. Wild-type cells showed low PI-3,5-P_2 amounts that significantly increased at least 10-fold during osmotic shock (Fig. 2*D*). In contrast, cells overexpressing Ivy1 showed a very modest increase in PI-3,5-P_2 levels under these conditions, in agreement with our microscopy analysis (Fig. 2 *A*–*C*). In contrast, we did not detect any significant difference in PI-3-P levels or other phosphoinositides between wild-type and cells overexpressing Ivy1 (Fig. S3*C*). We asked which role Ypt7 has on PI-3,5-P_2 regulation since Ivy1 requires Ypt7 for its localization (Fig. 1*A*). We measured PI-3,5-P_2 levels of *ypt7Δ* cells after hypertonic shock and observed a much lower increase than in wild-type cells, suggesting that Ypt7 acts upstream of the Fab1 complex (Fig. S1*E*). It is known that cells with impaired vacuole functionality are sensitive to growth in divalent cations (28–30). To address if Ivy1 overproduction has functional consequences, we grew cells on $ZnCl_2$ and observed reduced growth. This indicates that impaired vacuole fragmentation affects cell physiology, potentially compromising vacuole membrane integrity, which, in turn, affects vacuolar cation transporters and $ZnCl_2$ storage (31) (Fig. 2*E*). We conclude that Ivy1 directly prevents vacuole fission by dampening stress-induced PI-3,5-P_2 production when overexpressed, whereas loss of Ivy1 results in vacuole fragmentation.

Ivy1 Interacts Dynamically with Fab1 on Vacuoles. We next asked if Ivy1 acts on Fab1. Initially, we used the hyperactive *fab1** allele, which produces fragmented vacuoles (14) (Fig. 3 *A* and *B*).

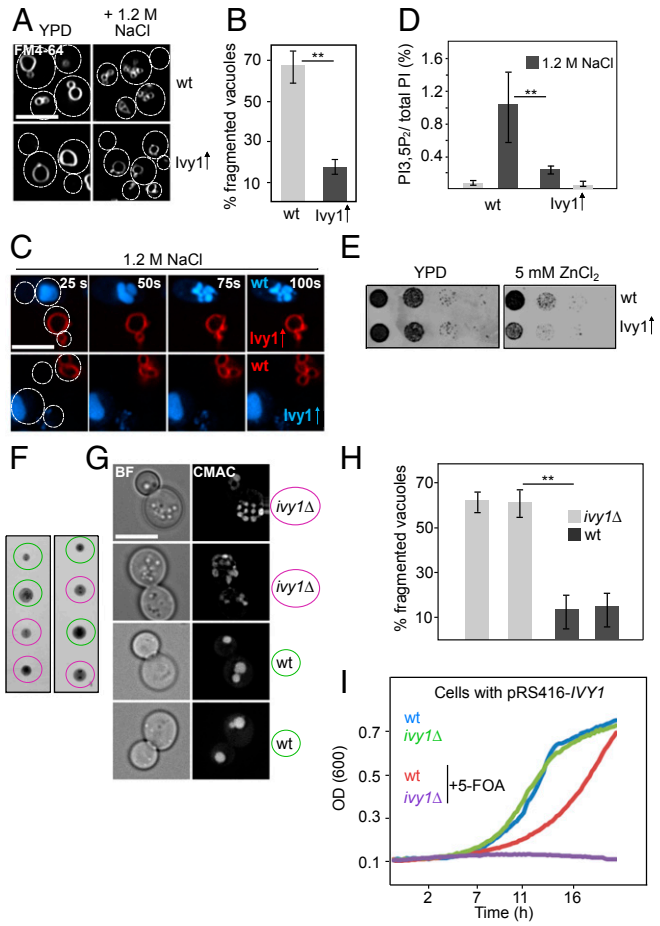

Fig. 2. A connection between Ivy1 and vacuole homeostasis. (*A*) A link between Ivy1 and osmotic stress. Ivy1 overexpression prevents vacuole fragmentation during osmotic stress. Indicated cells were FM4-64 stained (Fig. 1*A*). (*B*) Quantification, $n = 3$. Results are mean ± SD (>125 cells). (*C*) Time course of vacuole fragmentation. Time-lapse imaging of WT (CMAC-stained vacuoles, blue *Upper*; red, *Lower*) or cells overexpressing Ivy1 (FM4-64–stained vacuoles, red, *Upper*; blue, *Lower*) under hypertonic shock. Cells were grown in a flow chamber in SDC and exposed to SDC with 1.2 M NaCl. Pictures were taken at indicated times after salt exposure. (*D*) Ivy1 overexpression suppresses PI-3,5-P_2 production upon hypertonic stress. Indicated cells were grown in ^{3}H-inositol containing medium in the absence or presence of 1.2 M NaCl. After 15 min, lipids were deacylated and radioactive inositol head groups were resolved by HPLCy; $n = 4$. (*E*) Ivy1 overexpression compromises vacuole membrane homeostasis. Serial dilutions of indicated strains were spotted on YPD or YPD + 5 mM $ZnCl_2$ and imaged after 2 or 4 d at 30 °C. (*F*) Tetrad dissection. *IVY1* was deleted in diploid cells carrying a pRS416-*IVY1* plasmid and sporulated. Growth differences on YPD are due to presence of *ade2Δ* in the genotype. (*G*) Deletion of *IVY1* results in vacuole fragmentation. *ivy1Δ* or WT cells of indicated spores, each containing pRS416-*IVY1*, were grown in presence of 5-FOA overnight, and diluted back in complete medium without 5-FOA for at least 6 h. Vacuoles were stained with CMAC (*Materials and Methods*) and analyzed by fluorescence microscopy. (*H*) Quantification of three independent complete tetrades. Results are means ± SD. (*I*) Growth of *ivy1Δ* mutants is impaired. Cells were grown overnight in SDC and diluted back in the morning in SDC. In the evening, cells were washed twice either with SDC or SDC with 5-FOA and diluted to an OD of 0.1 in respective media. Cells were grown overnight at 30 °C, and OD was measured continuously using a plate reader (Molecular Devices). $^{**}P < 0.01$. (Scale bars: 5 μm.)

When Ivy1 was overproduced, the vacuole fragmentation was largely suppressed, suggesting a direct effect of Ivy1 on Fab1 activity. Ivy1 did so even in the absence of Fig4, supporting a model where Ivy1 inhibits Fab1 instead of activating Fig4 (Fig. S1 *F* and *G*). We measured the PI-3,5-P_2 levels and detected higher levels of PI-3,5-P_2 in the *fab1** allele, which increased even further under hypertonic conditions. However, Ivy1 overproduction strongly reduced this increase in PI-3,5-P_2 levels (Fig. 3*C*). The most plausible explanation would be a direct interaction between Ivy1 and Fab1. We used a bifluorescence complementation approach and attached the two halves of YFP, VN and VC, to Ivy1 and Fab1. We observed YFP-positive dots on vacuoles, similar to the native localization of Ivy1, whereas no signal was detectable between Vac8 and Ivy1 regardless of the combination (Fig. 3*D* and Fig. S2*E*). As a second approach, we tested for copurification of Ivy1 and Fab1. When cells expressing GFP-tagged Fab1 or Vac8 were subjected to anti-GFP pull down, we observed a clear interaction of Fab1-GFP with Ivy1 (Fig. 3*E*). Supporting this, mKate-tagged Ivy1 largely colocalized with Fab1-mNeonGreen on vacuoles; however, such a colocalization was not observed between Ivy1 and Vac8 (Fig. 3 *F* and *G*). If Ivy1 inhibits Fab1, we would expect that Ivy1 would separate from Fab1 during salt stress, when Fab1 activity increases. We monitored cells when exposed to salt stress as before (Fig. 2*C*), but now compared the relative distribution of Ivy1 and Fab1 (Fig. 3 *H* and *I*). In agreement with our hypothesis, Ivy1 separated from Fab1 within seconds as soon as cells were exposed to high salt, whereas it remained associated with Fab1 without salt stress (Fig. 3 *H* and *I*). This observation suggests that Ivy1 is a local and dynamic inhibitor of Fab1 activity on vacuoles.

Lateral Positioning of Ivy1 Is Critical for Localized Fab1 Inhibition. The dot-like positioning of Ivy1 suggests a locally confined inhibition of Fab1. We wondered if we could test this by redirecting Ivy1 to different microcompartments of the vacuole. For this, we attached the chromobody to GFP to several proteins that have been either colocalized with Ivy1 (Ego1, Fab1) or not (the V-ATPase subunit Vph1) (24, 32) (this work). CB tagging of these proteins or GFP tagging of Ivy1 did not affect vacuole morphology (Fig. 4 *A* and *F*), nor the response of these cells to osmotic stress (Fig. 4*E*) or normal growth (Fig. S3*D*). We tagged Ivy1 with GFP in cells carrying CB-tagged proteins and monitored vacuole morphology. When Ivy1-GFP was expressed in the Fab1-CB background, Ivy1 was found in dot-like structures. However, upon exposure to high salt, vacuole fragmentation was blocked, even when Ivy1 was not overexpressed (Fig. 4 *B* and *E*). In contrast, when Ego1 was GFP-tagged in the presence of Fab1-CB, vacuoles fragmented as in wild type, indicating that Fab1 functionality is not generally impaired by linking it to GFP-tagged protein (Fig. S3*B*). These findings agree with our in vivo observation that Ivy1 needs to separate from Fab1 under these conditions to release local inhibition of the kinase (Fig. 3*H*).

Strikingly, we observed the same vacuole fragmentation when wild-type Ivy1-GFP was coexpressed with Ego1-CB or Vph1-CB. This fragmentation phenotype was restored, when we introduced a plasmid coding for untagged Ivy1 (Fig. 4 *C* and *F*), indicating that the fragmentation is a consequence of the lateral relocalization of Ivy1. The observed fragmentation was not due to an interference with the fusion machinery since vacuoles became round after water treatment (Fig. 4*D*). To test if fragmentation is the result of linking Ivy1 to another protein complex, we tagged either Ego1 or the retromer subunit Vps35 with GFP in the Vph1-CB background. Both proteins localized to the vacuole but did not alter vacuole morphology (Fig. S3*A*). To test how relocalization affects physiology, we monitored growth of cells with laterally mistargeted Ivy1 on plates. Strikingly, cells with Ego1-targeted Ivy1 or Vph1-targeted Ivy1 grew very slowly (Fig. 4*G*), in agreement with the observed growth defect of the *ivy1Δ* cells (Fig. 2 *F* and *H*). We conclude that Ivy1 regulates Fab1 and maintains a functional vacuole during osmotic stress and normal growth.

Discussion

Here, we uncover Ivy1 as a sensor of vacuole membrane integrity that controls cell functionality during osmotic stress. Ivy1 binds directly to the vacuolar Fab1 complex and inhibits its activity. During hypertonic stress, Ivy1 relocalizes away from Fab1 on the

CELL BIOLOGY

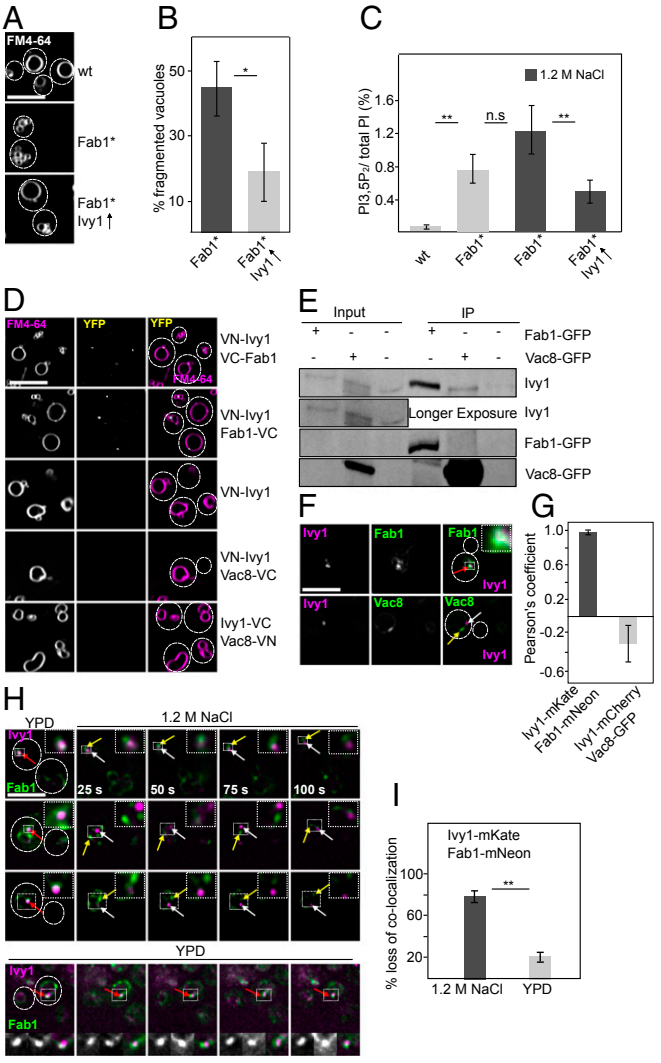

Fig. 3. Ivy1 directly regulates the Fab1 complex on the vacuole membrane. (*A*) Ivy1 suppresses a hyperactive *fab1* allele. Hyperactive *fab1* allele was introduced in *fab1Δ* cells, Ivy1 was overexpressed. Vacuole morphology was analyzed by FM4-64 staining (*Materials and Methods*). (*B*) Quantification, $n = 3$. Results are mean ± SD (>100 cells). (*C*) Ivy1 overexpression suppresses the PI-3,5-P_2 production of the *fab1* hyperactive allele upon hypertonic stress. PI-3,5-P_2 levels were measured as in Fig. 2*D*, $n = 3$. (*D*) Proximity of Ivy1 and Fab1 on vacuoles by Split-YFP. Ivy1 was N-terminally tagged with N-terminal half of the Venus (VN), Fab1 either N-terminally or C-terminally, and Vac8 was C-terminally tagged with VC and VN (45). Cells were monitored by fluorescence microscopy. (*E*) Physical interaction between Ivy1 and Fab1 on vacuoles. Vacuoles were isolated from strains expressing C-terminally GFP-tagged Fab1 or Vac8, lysed, and GFP-tagged proteins were isolated by GFP-TRAP beads (*Materials and Methods*). Bound proteins were resolved on SDS gels and analyzed by Western blotting. Fab1 was poorly detectable in the load fraction due to its low abundance. Input corresponds to 2.5% of lysate. (*F*) Colocalization of Ivy1 and Fab1 on vacuoles. Ivy1 and Fab1 were endogenously C-terminally tagged with mKate or mNeonGreen and analyzed by fluorescence microscopy. Ivy1 was C-terminally tagged with 3xmCherry and Vac8 C-terminally tagged with mGFP. (*G*) Pearson's correlation coefficient is shown. $n = 6$ (>400 cells). (*H*) Lateral segregation of Ivy1 and Fab1 on the vacuolar surface during hyperosmotic stress. Same cells as in *F* were monitored in a flow chamber before and after the exposure to 1.2 M NaCl in SDC. Time is given in seconds. (*I*) Quantification of loss of colocalization is shown at *Left*. Results are mean ± SD; $n = 3$ (>70 cells). $^*P < 0.05$, $^{**}P < 0.01$, n.s, nonsignificant. (Scale bars: 5 μm.)

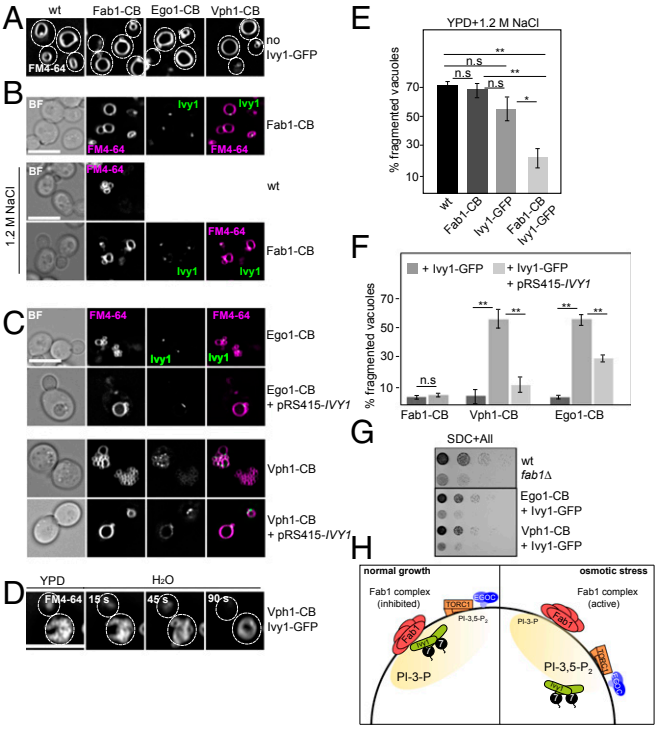

Fig. 4. Lateral relocalization of Ivy1 affects vacuole morphology and cell physiology. (*A*) Functionality of tagged subunits. Fab1, Ego1, and Vph1 were tagged C-terminally with a chromobody that specifically binds GFP. Vacuoles were FM4-64 stained and analyzed by fluorescence microscopy. (*B*) Effect of Ivy1 attachment to Fab1. Cells carrying Fab1-CB and expressing Ivy1-GFP were monitored as in *A* under normal and hypertonic conditions. BF, bright field. (*C*) Alteration of vacuole morphology upon lateral relocalization of Ivy1. Ivy1-GFP was expressed in cells carrying Ego1-CB and Vph1-CB, and vacuole morphology was analyzed as in *A* and *B*. (*D*) Fusion competence of fragmented vacuoles. Cells expressing Ivy1-GFP and Vph1-CB were FM4-64 stained and incubated in a flow chamber. At indicated times, the medium was replaced by H_2O and cells were monitored by fluorescence microscopy. (*E*) Quantification of vacuole morphology of indicated cells when exposed to hypertonic stress. Results are mean ± SD. $n = 3$ (>48 cells). (*F*) Quantification of vacuole fragmentation as observed in *B*–*D*. Results are mean ± SD. $n = 3$ (>48 cells). (*G*) Relocalization of Ivy1 impairs growth. Serial dilutions of indicated strains were spotted on SDC and imaged after 2 or 4 d at 30 °C. (*H*) Model of Ivy1 function. $^{**}P < 0.01$, $^*P < 0.05$, n.s, nonsignificant. (Scale bars: 5 μm.)

vacuole, relieving Fab1, which then produces PI-3,5-P_2 as a prerequisite of vacuole fragmentation (Fig. 4*H*). Supporting this, overproduction of Ivy1 blocks vacuole fragmentation, corrects the hyperactive *fab1** allele, and suppresses PI-3,5-P_2 production during hyperosmotic stress. This important role of Ivy1 can be mirrored if we laterally relocalize Ivy1 with the chromobody attached to selected vacuolar proteins, indicating that lateral localization into microcompartments on the vacuolar membrane is of functional importance. Furthermore, *ivy1Δ* mutants present fragmented vacuoles and reduced growth.

How does Ivy1 respond and detect membrane stress? We can only speculate on its precise function. Ivy1 has a central I-BAR domain, which is critical for its function (24). It can oligomerize on membranes in vitro, yet requires Ypt7 for its localization (24) and function. It also binds two signature lipids of the vacuole, PI-3-P and PI-3,5-P_2. It has all required properties of an organelle membrane sensor that detects alterations in membrane packing or its homeostasis. While such a function remains to be shown, the lateral relocalization of Ivy1 away from Fab1 during hypertonic stress strongly favors this idea. This possible function of Ivy1 as a membrane sensor would be reminiscent of the function of the plasma membrane Slm1 in yeast, which activates the

TORC2 complex and promotes the synthesis of sphingolipids (33). Ivy1, like Slm1, could directly translate alterations in membrane organization into a signaling process that corrects for this defect. Future experiments need to test if such a model applies. Of interest, another Rab7 effector has recently been identified that controls PI-3-P levels on endosomes by inhibiting the PI-3-P kinase complex, suggesting that local inhibition of lipid kinase complexes may be a common scheme (34).

Modulation of Fab1 by Ivy1 adds to the complexity of its regulation. Fab1 is part of a complex, which includes the Fig4 PI-3-P 5-phosphatase, the adapter Vac14, the membrane protein Vac7, and the propeller Atg18 (20, 21). While deletion of single subunits of the complex reveals roles for each subunit on Fab1 localization and its resulting activity, it has remained a challenge to determine their direct roles due to complex regulatory networks. One striking example is Atg18, where the deletion causes both very high Fab1 activity and large vacuoles (21–23). In this regard, the analysis of Ivy1 marks an important advance as we are able to modulate vacuole morphology depending on Ivy1 expression and localization, and can directly detect reduced Fab1 activity upon Ivy1 overexpression. Our data agree with a direct binding of Ivy1 to Fab1 as a local inhibitor, although we cannot exclude other interactions within the complex. It is possible that Ivy1 directly controls the available PI-3-P pool around Fab1 and only makes this available when Fab1 activity is required, although the PI-3-P levels were unchanged upon Ivy1 overexpression. It is noteworthy that vacuole membranes segregate into distinct domains during starvation or upon alteration of its ergosterol content (32, 35, 36). Ivy1 segregates into these domains during heat stress or starvation (24, 32). The lateral separation of Ivy1 and Fab1 may take advantage of possible transient domain formations during osmotic stress.

Why has Ivy1 function been overlooked? In our initial analyses, we uncovered Ivy1 as a membrane modulator and Ypt7 interactor and observed a response of Ivy1 to membrane stress. However, the deletion showed no apparent morphology defect. Only in combination with a V-ATPase deletion, vacuole membranes expanded strongly without further volume increase (24). Our genetic analysis of Ivy1 now reveals that *ivy1*Δ cells are suppressed by another mutation. Upon segregation, *ivy1*Δ cells grew extremely slow and had fragmented vacuoles (Fig. 2*G*), although we could not measure PI-3,5-P_2 levels due to the slow growth (Fig. 2*I*), and the easy acquisition of suppressors. Identification of the suppression mechanism will provide additional insights into the control of vacuolar membrane homeostasis. Importantly, we also observed fragmentation of vacuoles when we depleted Ivy1 (Fig. S2 *A* and *B*). Ivy1 function is thus far more critical for vacuole biogenesis and yeast cell survival than anticipated.

Lysosomal function depends on PI-3,5-P_2 homeostasis, as revealed by the strong neurological phenotypes upon loss of the PIKfyve kinase and Fig4 phosphatase activities in metazoans (12). Both the V-ATPase and the TORC1 complex are modulated by the lipid environment (6, 7, 37), and cells lacking the Fab1 complex have growth defects. A precise understand of PI-3,5-P_2 function on vacuoles will be important for our further understanding of vacuole biogenesis in general.

Materials and Methods

Yeast Genetic Manipulation and Molecular Biology. *Saccharomyces cerevisiae* strains used are listed in Table S1. Genetic manipulations were made by homologous recombination of PCR fragments as described previously (38, 39). Ivy1 point mutants were generated by QuikChange mutagenesis. Truncations were generated using primers aligning at the desire region and introduced a restriction site. PCR product was digested and ligated into plasmids. All plasmids are listed in Table S2.

Light Microscopy and Image Analysis. Cells were grown to log-phase in yeast extract peptone (YP) medium containing glucose (YPD), galactose (YPG), or synthetic medium supplemented with essential amino acids (SDC). Vacuole membrane was stained with 30 μM FM4-64 for 30 min, followed by washing with medium, and incubation in medium without dye for 1 h before analysis (40). For luminal staining of vacuoles, cells were incubated in 0.1 mM 7-amino-4-chloromethylcoumarin (CMAC) for 10 min and washed with SDC. Images were acquired on an Olympus IX-71 inverted microscope equipped with a 100× N.A. 1.49 objective, an sCMOS camara (PCO), an InsightSSI illumination system, and SOftWoRx software (Applied Precision). Images were processed with ImageJ. One representative plane of a z-stack is shown unless noted.

Purification of Recombinant Proteins. *Escherichia coli* BL21 (DE3) Rosetta cells containing the *IVY1* or *YPT7/VPS21* plasmids were grown to optical density 600 (OD_{600}) of 0.8. Expression was induced with 0.5 mM IPTG overnight at 16 °C. Cells were harvested and lysed in 50 mM Tris·HCl, pH 7.5, 150 mM NaCl, 1 mM PMSF, 1× protease inhibitor mixture (1× = 0.1 mg/mL leupeptin, 1 mM *o*-phenanthroline, 0.5 mg/mL pepstatin A, 0.1 mM Pefabloc). Lysates were centrifuged 15 min at 30,000 × *g*, cleared supernatant was added to Ni-NTA beads for His-tagged protein or to GSH-beads for GST-tagged protein, followed by incubation for 1 h at 4 °C. Ni-NTA beads were washed with 25 mL of buffer containing 0.02 M imidazole. His-Ivy1 was eluted from beads with buffer containing 0.3 M imidazole. GST-tagged proteins were eluted with buffer containing 15 mM reduced glutathione. Proteins were desalted into 50 mM Tris·HCl, pH 7.5, 150 mM NaCl, 1 mM PMSF, 1× protease inhibitor mixture, 5% (vol/vol) glycerol buffer using a Slide A Dialysis Cassette, 10,000 molecular weight cutoff (Thermo Scientific), snap frozen, and stored at −80 °C until further use.

Rab GTPase Pull-Down. Recombinant GST-Rabs were loaded with 1 mM GDP or GTPγS in 20 mM Hepes/NaOH, pH 7.4. One hundred fifty-microgram Rabs were coupled to GSH beads. Rabs were incubated with recombinant His-Ivy1 (or control proteins) for 1 h at 4 °C. Beads were washed three times with 20 mM Hepes/NaOH, pH 7.4, 100 mM NaCl, 1 mM $MgCl_2$, 0.1% (wt/vol) Triton X-100; proteins were eluted with 20 mM Hepes/NaOH, pH 7.4, 100 mM NaCl, 1 mM $MgCl_2$, 0.1% (wt/vol) Triton X-100, 20 mM EDTA. Eluates were precipitated with tricloracetic acid (TCA), analyzed by SDS/PAGE and Western blotting. As loading control, bound Rabs were eluted from the beads by boiling in sample buffer and analyzed by SDS/PAGE and Coomassie staining.

Growth Test. Cells were grown to log-phase, washed twice with SDC, and diluted to an OD_{600} of 0.25. Serial dilutions (1:10) were spotted onto plates and imaged after 2–4 d. For growth curves, cells were grown to logarithmic phase in SDC, washed twice either with SDC or SDC plus the drug to be tested, and diluted to an OD_{600} of 0.1. Cells were grown overnight at 30 °C in a 96-well plate, and OD was measured using a plate reader (Molecular Devices).

Liposome Flotation Assay. A film of dried lipids was prepared by chloroform evaporation (41). Once dried, the film was resuspended in HK buffer (50 mM Hepes/KOH, pH 7.2, 120 mM KOAc). The suspension was subjected to five freeze-thaw cycles and afterward extruded through polycarbonate filters (pores 0.4, 0.2, 0.05, 0.03 μm). The following vacuole-like composition was used (in mol%): dioleoylphosphatidyl choline (DOPC; 51.9), dioleoylphosphatidylethanolamine (DOPE; 18), Soy phosphatidylinositol (SoyPI, 18), cardiolipin (1.6), ergosterol (8), diacylglycerol (DAG; 1), Rhodamine B 1,2-dihexadecanoyl-*sn*-glycero-3-phosphoethanolamine (rh-DHPE; 1.5). For the PA-containing liposomes: DOPC (49.9), DOPE (18), SoyPI (18), dioleoylphosphatidic acid (PA, 2), cardiolipin (1.6), ergosterol (8), DAG (1), rh-DHPE (1,5). For the PI-3-P liposomes: DOPC (50.9), DOPE (18), SoyPI (18), cardiolipin (1.6), ergosterol (8), DAG (1), rh-DHPE (1.5), PI-3-P (1). For the PI-4-P liposomes: DOPC (50.9), DOPE (18), SoyPI (18), cardiolipin (1.6), ergosterol (8), DAG (1), rh-DHPE (1.5), PI-4-P (1). And for the PI-3,5-P_2 liposomes: DOPC (50.9), DOPE (18), SoyPI (18), cardiolipin (1.6), ergosterol (8), DAG (1), rhDHPE (1.5), PI-3,5-P_2 (1). For the flotation, proteins were incubated with liposomes in 150 μL of HKM buffer (HK buffer with 1 mM $MgCl_2$) at room temperature for 10 min. Suspension was adjusted to 30% sucrose by mixing 100 μL of 75% (wt/vol) sucrose solution in HKM buffer, overlaid with 200 μL containing 25% sucrose and 50 μL of sucrose-free HKM. Samples were centrifuged in a swinging rotor (SW40) for 1 h at 100,000 × *g*. Top fractions were collected (80 μL) and analyzed by Western blotting.

Vacuole Isolation and Coimmunoprecipitation. Vacuoles were isolated as described (42). A P13 fraction was prepared from strains expressing Vac8-GFP, Fab1-GFP, or no GFP-tagged protein using published protocols (43). Once isolated, vacuoles were lysed in buffer containing 20 mM Hepes/KOH, pH 7.4, 150 mM KAc, 5% glycerol (vol/vol), 25 mM CHAPS, and a protease inhibitor mixture mention above, incubated on a turning wheel for 30 min at 4 °C. Lysate was centrifuged for 10 min at 20,000 × *g* at 4 °C; supernatant was incubated with GFP-Trap beads (Chromotek) for 1 h. Beads were washed twice with lysis buffer, boiled in sample buffer, and eluted proteins were analyzed by Western Blotting.

Tetrad Analysis. Yeast strains with different mating types were streaked out on a double-selective plate to allow mating and diploid cell selection. Diploid cells were cultured in YPD overnight to a stationary phase, pelleted, resuspended in residual medium, and plated as one drop onto potassium acetate plates [2% potassium acetate (wt/vol) and 2% agar (wt/vol)]. After 3 d, cells were dissolved in 100 μL of sterile water with zymolyase (MP Biomedicals) and incubated for 10 min at room temperature. Twenty microliters were streaked out onto a YPD plate, tetrads were separated with a micromanipulator, and grown for at least 3 d. Genotype of the spores was determined by testing growth on selective media.

Phosphoinositide Analysis. Analysis of cellular phosphoinositide levels was performed as previously described (44) with the following modifications. Midlog cells (5 OD_{600} equivalents) grown in yeast nitrogen base media were harvested, washed in inositol free media (IFM), incubated for 10 min in inositol-free media, and labeled with *myo*-[2-^{3}H] inositol (PerkinElmer) for 30 min. Following this initial labeling, cultures were split and further incubated in IFM or IFM containing 1.2 M NaCl for 15 min. Cells were precipitated in 4.5% perchloric acid and lysed by vortexing with glass beads. Cell lysates were washed in 100 mM EDTA, phospholipids were deacylated, and further processed as previously described (44). Samples were dried and resuspended in H_2O. Identification and quantitation of ^{3}H-labeled glycerolphosphoinositols was performed by HPLCy (HPLC) using a Series 200 HPLC system (PerkinElmer), a partisphere SAX column (HiChrom), an inflow 150TR radiomatic detector (PerkinElmer), TCNav software, and TotalChrom workstation (PerkinElmer). Data for individual phosphoinositide species data are shown as percentages of the total number of counts detected for normalization.

ACKNOWLEDGMENTS. We thank Claudio De Virgilio and Florian Fröhlich for discussion, Jürgen Heinisch for support, Roland Wedlich-Söldner for plasmids, and Kathrin Auffarth and Angela Perz for excellent technical assistance. This work was supported by DFG Grant UN111/10-1 (to C.U.), and by Medical Research Council (MRC) funding to the MRC Laboratory for Molecular Cell Biology, University College London, Award MC_UU_12018/6 (to C.J.S.). P.C.M. received additional support by the graduate program of the Collaborative Research Center 944 (SFB 944).

1. Schink KO, Tan K-W, Stenmark H (2016) Phosphoinositides in control of membrane dynamics. *Annu Rev Cell Dev Biol* 32:143–171.
2. Barr FA (2013) Review series: Rab GTPases and membrane identity: Causal or inconsequential? *J Cell Biol* 202:191–199.
3. Huotari J, Helenius A (2011) Endosome maturation. *EMBO J* 30:3481–3500.
4. Odorizzi G, Babst M, Emr S (1998) Fab1p PtdIns(3)P 5-kinase function essential for protein sorting in the multivesicular body. 95:847–858.
5. Dong X-P, et al. (2010) PI(3,5)P(2) controls membrane trafficking by direct activation of mucolipin Ca(2+) release channels in the endolysosome. *Nat Commun* 1:38.
6. Bridges D, et al. (2012) Phosphatidylinositol 3,5-bisphosphate plays a role in the activation and subcellular localization of mechanistic target of rapamycin 1. *Mol Biol Cell* 23:2955–2962.
7. Jin N, et al. (2014) Roles for PI(3,5)P2 in nutrient sensing through TORC1. *Mol Biol Cell* 25:1171–1185.
8. Gary JD, Wurmser AE, Bonangelino CJ, Weisman LS, Emr SD (1998) Fab1p is essential for PtdIns(3)P 5-kinase activity and the maintenance of vacuolar size and membrane homeostasis. *J Cell Biol* 143:65–79.
9. Lang MJ, Strunk BS, Azad N, Petersen JL, Weisman LS (2017) An intramolecular interaction within the lipid kinase Fab1 regulates cellular phosphatidylinositol 3,5-bisphosphate lipid levels. *Mol Biol Cell* 28:858–864.
10. McCartney AJ, et al. (2014) Activity-dependent PI(3,5)P2 synthesis controls AMPA receptor trafficking during synaptic depression. *Proc Natl Acad Sci USA* 111: E4896–E4905.
11. Bharadwaj R, Cunningham KM, Zhang K, Lloyd TE (2015) FIG4 regulates lysosome membrane homeostasis independent of phosphatase function. *Hum Mol Genet* 25: 681–692.
12. Zolov SN, et al. (2012) In vivo, PIKfyve generates PI(3,5)P2, which serves as both a signaling lipid and the major precursor for PI5P. *Proc Natl Acad Sci USA* 109: 17472–17477.
13. Zhang Y, et al. (2012) Modulation of synaptic function by VAC14, a protein that regulates the phosphoinositides PI(3,5)P_2 and PI(5)P. *EMBO J* 31:3442–3456.
14. Gary JD, et al. (2002) Regulation of Fab1 phosphatidylinositol 3-phosphate 5-kinase pathway by Vac7 protein and Fig4, a polyphosphoinositide phosphatase family member. *Mol Biol Cell* 13:1238–1251.
15. Rudge SA, Anderson DM, Emr SD (2004) Vacuole size control: Regulation of PtdIns(3,5)P2 levels by the vacuole-associated Vac14-Fig4 complex, a PtdIns(3,5)P2-specific phosphatase. *Mol Biol Cell* 15:24–36.
16. Rusten TE, et al. (2006) Fab1 phosphatidylinositol 3-phosphate 5-kinase controls trafficking but not silencing of endocytosed receptors. *Mol Biol Cell* 17:3989–4001.
17. Bonangelino CJ, et al. (2002) Osmotic stress-induced increase of phosphatidylinositol 3,5-bisphosphate requires Vac14p, an activator of the lipid kinase Fab1p. *J Cell Biol* 156:1015–1028.
18. McCartney AJ, Zhang Y, Weisman LS (2014) Phosphatidylinositol 3,5-bisphosphate: Low abundance, high significance. *BioEssays* 36:52–64.
19. Duex JE, Tang F, Weisman LS (2006) The Vac14p-Fig4p complex acts independently of Vac7p and couples PI3,5P2 synthesis and turnover. *J Cell Biol* 172:693–704.
20. Botelho RJ, Efe JA, Teis D, Emr SD (2008) Assembly of a Fab1 phosphoinositide kinase signaling complex requires the Fig4 phosphoinositide phosphatase. *Mol Biol Cell* 19: 4273–4286.
21. Jin N, et al. (2008) VAC14 nucleates a protein complex essential for the acute interconversion of PI3P and PI(3,5)P_2 in yeast and mouse. *EMBO J* 27:3221–3234.
22. Efe JA, Botelho RJ, Emr SD (2007) Atg18 regulates organelle morphology and Fab1 kinase activity independent of its membrane recruitment by phosphatidylinositol 3,5-bisphosphate. *Mol Biol Cell* 18:4232–4244.
23. Dove SK, et al. (2004) Svp1p defines a family of phosphatidylinositol 3,5-bisphosphate effectors. *EMBO J* 23:1922–1933.
24. Numrich J, et al. (2015) The I-BAR protein Ivy1 is an effector of the Rab7 GTPase Ypt7 involved in vacuole membrane homeostasis. *J Cell Sci* 128:2278–2292.
25. Lürick A, et al. (2017) Multivalent Rab interactions determine tether-mediated membrane fusion. *Mol Biol Cell* 28:322–332.
26. Lazar T, Scheglmann D, Gallwitz D (2002) A novel phospholipid-binding protein from the yeast Saccharomyces cerevisiae with dual binding specificities for the transport GTPase Ypt7p and the Sec1-related Vps33p. *Eur J Cell Biol* 81:635–646.
27. Nishimura K, Fukagawa T, Takisawa H, Kakimoto T, Kanemaki M (2009) An auxin-based degron system for the rapid depletion of proteins in nonplant cells. *Nat Methods* 6:917–922.
28. Woolford CA, Bounoutas GS, Frew SE, Jones EW (1998) Genetic interaction with vps8-200 allows partial suppression of the vestigial vacuole phenotype caused by a pep5 mutation in Saccharomyces cerevisiae. *Genetics* 148:71–83.
29. Srivastava A, Woolford CA, Jones EW (2000) Pep3p/Pep5p complex: A putative docking factor at multiple steps of vesicular transport to the vacuole of Saccharomyces cerevisiae. *Genetics* 156:105–122.
30. Paulsel AL, Merz AJ, Nickerson DP (2013) Vps9 family protein Muk1 is the second Rab5 guanosine nucleotide exchange factor in budding yeast. *J Biol Chem* 288: 18162–18171.
31. MacDiarmid CW, Milanick MA, Eide DJ (2003) Induction of the ZRC1 metal tolerance gene in zinc-limited yeast confers resistance to zinc shock. *J Biol Chem* 278: 15065–15072.
32. Toulmay A, Prinz WA (2013) Direct imaging reveals stable, micrometer-scale lipid domains that segregate proteins in live cells. *J Cell Biol* 202:35–44.
33. Berchtold D, et al. (2012) Plasma membrane stress induces relocalization of Slm proteins and activation of TORC2 to promote sphingolipid synthesis. *Nat Cell Biol* 14: 542–547.
34. Araki Y, et al. (2013) Atg38 is required for autophagy-specific phosphatidylinositol 3-kinase complex integrity. *J Cell Biol* 203:299–313.
35. Tsuji T, et al. (2017) Niemann-Pick type C proteins promote microautophagy by expanding raft-like membrane domains in the yeast vacuole. *eLife* 6:e25960.
36. Seo AY, et al. (2017) AMPK and vacuole-associated Atg14p orchestrate μ-lipophagy for energy production and long-term survival under glucose starvation. *eLife* 6: e21690.
37. Li SC, et al. (2014) The signaling lipid PI(3,5)P_2 stabilizes V_1-V(o) sector interactions and activates the V-ATPase. *Mol Biol Cell* 25:1251–1262.
38. Janke C, et al. (2004) A versatile toolbox for PCR-based tagging of yeast genes: New fluorescent proteins, more markers and promoter substitution cassettes. *Yeast* 21: 947–962.
39. Longtine MS, et al. (1998) Additional modules for versatile and economical PCR-based gene deletion and modification in Saccharomyces cerevisiae. *Yeast* 14:953–961.
40. Vida TA, Emr SD (1995) A new vital stain for visualizing vacuolar membrane dynamics and endocytosis in yeast. *J Cell Biol* 128:779–792.
41. Cabrera M, et al. (2010) Phosphorylation of a membrane curvature-sensing motif switches function of the HOPS subunit Vps41 in membrane tethering. *J Cell Biol* 191: 845–859.
42. Haas A, Scheglmann D, Lazar T, Gallwitz D, Wickner W (1995) The GTPase Ypt7p of Saccharomyces cerevisiae is required on both partner vacuoles for the homotypic fusion step of vacuole inheritance. *EMBO J* 14:5258–5270.
43. LaGrassa TJ, Ungermann C (2005) The vacuolar kinase Yck3 maintains organelle fragmentation by regulating the HOPS tethering complex. *J Cell Biol* 168:401–414.
44. Manford AG, Stefan CJ, Yuan HL, Macgurn JA, Emr SD (2012) ER-to-plasma membrane tethering proteins regulate cell signaling and ER morphology. *Dev Cell* 23:1129–1140.
45. Sung M-K, Huh W-K (2007) Bimolecular fluorescence complementation analysis system for in vivo detection of protein-protein interaction in Saccharomyces cerevisiae. *Yeast* 24:767–775.